Applied Surface Science 290 (2014) 180–187

Contents lists available at ScienceDirect

Applied Surface Science

journal homepage: www.elsevier.com/locate/apsusc

# Ultrathin (0 0 1) and (1 0 0) $TiO_2$(B) sheets: Surface reactivity and structural properties

Luciana Fernández-Werner[a,b,c], Ricardo Faccio[a,b,c,*], Alfredo Juan[d], Helena Pardo[a,b,c], Benjamín Montenegro[a,b,c], Álvaro W. Mombrú[a,b,c]

[a] Cryssmat-Lab, DETEMA, Facultad de Química, Universidad de la República, Montevideo, Uruguay
[b] Centro NanoMat, Cryssmat-Lab, DETEMA, Polo Tecnológico de Pando, Facultad de Química, Universidad de la República, Cno. Saravia s/n, Pando, Uruguay
[c] Centro Interdisciplinario en Nanotecnología, Química y Física de Materiales (CINQUIFIMA), Espacio Interdisciplinario, Universidad de la República, Montevideo, Uruguay
[d] Departamento de Física, Universidad Nacional del Sur, Av. Alem 1253, Bahía Blanca 8000, Argentina

ARTICLE INFO

*Article history:*
Received 6 August 2013
Accepted 7 November 2013
Available online 18 November 2013

*Keywords:*
$TiO_2$(B)
Ultrathin sheets
Formic acid
DFT

ABSTRACT

B polymorph of titanium dioxide ($TiO_2$(B)) appears as a metastable phase during thermal annealing of low content sodium layered titanate nanostructures obtained via the widely used hydrothermal synthesis. In addition, the computed formation energy for the $TiO_2$(B) (0 0 1) slabs in the order of the one calculated for anatase (1 0 1) which represents one of the most stable $TiO_2$ surfaces. This encourages the study of this polymorph which could gain prominence in $TiO_2$ applications at the nanoscale.

In a first instance ultrathin $TiO_2$(B) sheets, parallel to crystallographic planes (0 0 1) and (1 0 0), are investigated and compared to other well know $TiO_2$ polymorphs, such as rutile and anatase surfaces. Then the adsorption of formic acid on (0 0 1) and (1 0 0) – less stable – $TiO_2$(B) dry ultrathin sheets was studied as the first step for further evaluation of $TiO_2$(B) nanostructures for dye sensitized solar cells (DSSC) applications. The results show that the monodentate through the carbonyl group configuration is the most stable for (0 0 1) sheet while bidentate dissociated configuration is the most stable for (1 0 0) sheet being the computed adsorption energies 0.51 eV and 1.49 eV, respectively. The evaluated reactivity of $TiO_2$(B) slabs is comparable with anatase and indicates that it could be a good adsorbent for common dyes used for dye sensitized solar cells purposes.



## 1. Introduction

$TiO_2$ has been exhaustively investigated due to its unique properties and wide range of well-known novel applications [1]. Most of the work has been focusing on anatase and rutile polymorphs owing to their comparative higher natural abundance, followed by brookite phase. Recently, $TiO_2$(B) polymorph has gained more attention due to its potential applications, mainly in rechargeable lithium ion batteries [2,3] but also in dye sensitized solar cells (DSSCs) [4,5] and supercapacitors [6].

$TiO_2$(B) was first synthesized by Marchand et al. [7], its chemical structure presents the host framework of the bronze $Na_xTiO_2$, exhibiting continuous channels and lower density than the other mentioned polymorphs. It can be easily obtained by soft chemical routes via proton exchange and subsequently dehydration of layered titanates as was then investigated by Feist and coworkers [8,9]. It was later observed by several groups during the annealing of samples obtained performing alkali hydrothermal synthesis, first introduced by the Kasuga et al. [10], of titania derived nanotubes [11]. Using this approach there were synthesized different $TiO_2$(B) nanostructural morphologies as nanoparticles [5], nanowires [2,3,6], nanoribbons [4] and nanotubes [12]. Regarding their performance on dye sensitized solar cells (DSSC), at the best of our knowledge, only a few evaluations have been reported [4,5,13] showing comparative results.

Some theoretical studies have also been carried out about this phase. Bulk structural, electronic and vibrational properties have been investigated by Ben Yahia M. and coworkers by means of first-principles density functional theory calculations [14]. Surface reconstruction and structural stability have been studied by Vittadini et al. [15]. In addition, Liu et al. have studied water adsorption on $TiO_2$(B) (0 0 1) and (1 0 0) facets [16]. Moreover, lithium transport has been evaluated by Arrouvel et al. [17].

The presence of $TiO_2$(B) during the synthesis of titania nanostructures, showing its comparatively stability with anatase at the nanoscale, together with the relatively low investigation, motivates this study in which we intent to contribute to the knowledge about understanding of this polymorph and their related low

* Corresponding author. Tel.: +598 2924 9859; fax: +598 2924 1906.
*E-mail addresses:* rfaccio@fq.edu.uy, rjfaccio@gmail.com (R. Faccio).

0169-4332/$ – see front matter © 2013 Elsevier B.V. All rights reserved.
http://dx.doi.org/10.1016/j.apsusc.2013.11.029

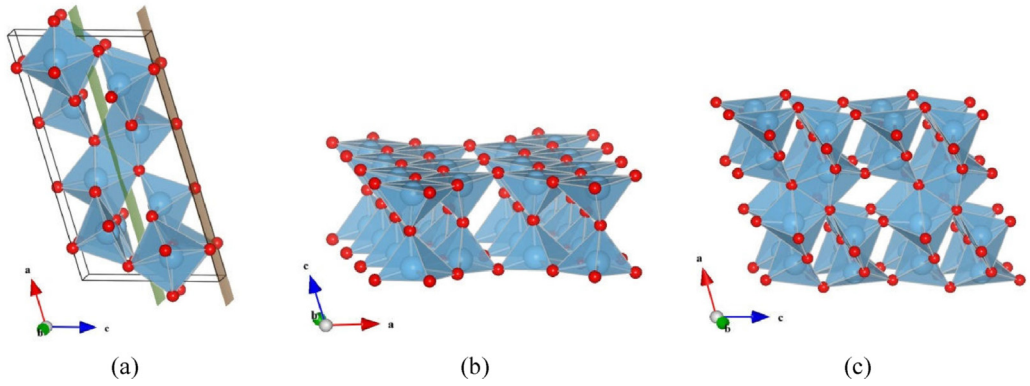


**Fig. 1.** $TiO_2$(B) unit cell showing the two cutting options along the direction (0 0 1) (a), TB (0 0 1) chosen slab with *c* as vacuum direction (b), and TB (1 0 0) slab with *a* as vacuum direction (c).

dimensional structures. Furthermore, as far as we know, there are no theoretical reports on its optical properties, and the implications in their use for potential DSSC applications. As a first approach, the information about HCOOH adsorption configurations provides relevant data about the geometry of interaction with ruthenium based complexes which have carboxylic groups as bending groups, extensively used as dyes for DSSC.

Regarding the selected bidimensional models, the focus on ultrathin sheets is due to the fact that there are several reports where titania and titanate nanotubes appears as scroll-like type structure, suggesting the rolling up of material sheets of few atomic planes of thickness. There are also observations of this kind of unrolling sheets coexisting with nanotubes as products [18,19]. In addition, ultrathin sheets have been successfully obtained via unrolling of nanotubes [20] or directly synthethized for various polymorphs $Ti_{1-\delta\square\delta}O_2^{4\delta-}$(~6 Å) [21,22], $Ti_4O_9$,$Ti_5O_{11}$ [23] and $TiO_2$(B) (~10-12 Å) [24,25]. We consider these kind of ultrathin surfaces are best suited for understanding the behavior of nanotubes and nanostructures, because of size and growth mechanism, in comparison with thick slab converged surfaces. Regarding $TiO_2$(B) nanotubes, there are evidences which suggest the surface (0 0 1) as exposed wall surface [26], but also surfaces (2 0 0) and (1 1 0) are proposed [27,28].

In this paper, ultrathin sheets of $TiO_2$(B) cutting along (0 0 1) and (1 0 0) crystallographic planes (TB (0 0 1) and TB (1 0 0) respectively) were optimized and evaluated, discussing its electronic properties. Additionally, the interaction between ultrathin sheets of $TiO_2$(B) with formic acid molecules were analyzed, comparing the adsorption energies for several different configurations including non-dissociative and dissociative chemisorption. The aim of this work is to provide more information concerning the electronic structure, stability and reactivity of this polymorph. We consider that this information is important to dimension the technological applications of these semiconductors in DSSC technologies.

## 2. Computational details and methodology

### 2.1. Ultrathin $TiO_2$(B) sheets, structural and electronic optimization

Density functional theory (DFT) calculations [29,30] were performed for the study of structural and electronic properties for $TiO_2$ bulk and ultrathin sheets structures using the projector-augmented wave (PAW) method [31,32] as implemented in the Vienna ab initio simulation package(VASP) [33]. An energy cutoff of 400 eV was used to expand the Kohn–Sham orbitals into plane wave basis sets. In addition to the 3d and 4s valence states, the 3s and 3p semicore states of Ti have been explicitly treated as valence states throughout this work. We selected the generalized gradient approximation (GGA) exchange–correlation (XC) functional according to Perdew–Burke–Ernzerhof (PBE) [34,35]. In all of the calculations reported here the *k*-point mesh was taken equivalent to $4 \times 4 \times 1$ for the full (reducible) Brillouin zone, allowing the convergence of total energy and forces.

The slabs were constructed by transformation of the unit cell followed by the application of a vacuum region, along the non-periodical direction, of about 10 Å which is sufficient to avoid significant interactions between different images of the slabs. We selected the following slabs for simulating the ultrathin sheets: anatase A (1 0 1), anatase A (1 0 0), anatase A (0 0 1), rutile R (1 0 0), rutile R (1 1 0), rutile R (1 0 1), $TiO_2$(B) TB (0 0 1) in one of the possible choices and $TiO_2$(B) TB (1 0 0), see Fig. 1 [36]. Both supercell dimensions and ions positions were allowed to optimize, until residual forces and stress tensor components were positioned down to 0.02 eV/Å and 5 kbar respectively. Well-known anatase and rutile polymorphs slabs were included in this point as comparative models.

### 2.2. Formic acid adsorption on clean (0 0 1) and (1 0 0) $TiO_2$(B) facets

The adsorption energies ($E_{form}$) were calculated according to the expression (i). $E_T$ stands for total energy calculated for the interacting $TiO_2$ slab and HCOOH molecule at the surface. $E_{ni}$ represents the total energy calculated for non-interacting slab and HCOOH molecule computed placing an isolated *trans* formic acid molecule far from the surface slab.

$$E_{form} = -(E_T - E_{ni}) \quad \text{(i)}$$

The thicknesses of sheets were chosen as the minimum unit as it appears in the corresponding bulk unit cells, and then vacuum was applied in the normal direction of the selected facets. These are $c\cos(\beta - 90^\circ) = 6.24$ Å for (0 0 1) and $a\cos(\beta - 90^\circ) = 11.64$ Å for (1 0 0) which implies a bilayer of Ti atoms in the first case and four layers of Ti in the second one, see Fig. 1.

In order to study the surface–HCOOH interaction, the molecule was situated in *trans* conformation on top of the $TiO_2$ layer. The selection of the *trans* isomer is based on the relatively favorable stability in comparison to the cis isomer in terms of total energy. The initial Ti(5c)–O distances are about 2.0–2.2 Å for each configuration, while for O(2c)–*H* distances are 1.7–2.0 Å and 1.1–1.4 Å for non-dissociated and dissociated respectively. Ti(5c) and O(2c) refers to the surface five-fold coordinated Ti and two-fold coordinated O respectively.

**Table 1**
Equivalent surface energies and energy gaps for the simulated slabs.

| Slabs | No. of atoms | $TiO_2$ layers | ESFE (J/m$^2$) | $E_g$ (eV) |
|---|---|---|---|---|
| **A (1 0 1)** | 8 | **2** | **0.41** | **2.86** |
| A (1 0 0) | 12 | 2 | 0.64 | 2.29 |
| A (0 0 1) | 15 | 5 | 0.93 | 2.12 |
| **R (1 1 0)** | 6 | **3** | **0.64** | **1.53** |
| R (1 0 1) | 6 | 3 | 1.07 | 1.87 |
| R (1 0 0) | 27 | 3 | 0.66 | 1.99 |
| **TB (0 0 1)** | 24 | **2** | **0.38** | **2.61** |
| TB (1 0 0) | 8 | 4 | 0.83 | 2.80 |

## 3. Result and discussion

### 3.1. Ultrathin sheets

Due to structural differences in $TiO_2$ polymorphs, different number of atoms was considered in each supercell. This information is included in Table 1, Fig. 1 and Fig. 2, in which the cutting planes along different lattices planes are shown. When comparing bulk structures, $TiO_2$(B) presents some of the titanium atoms with distorted square–pyramidal instead of octahedral coordination polyhedra as expected for rutile and anatase, see Fig. 1. The computed distance $d_{Ti-O}$ = 2.34 Å is greater than typical Ti–O single bond length (2.20–2.25 Å), this result is in agreement with previous observations [14,15] where the relative stability of the different facets are based on this fact.

The equivalent surface formation energy (ESFE), corresponding to the formation energy of the ultrathin slabs per unit area, (shown in Table 1) were determined using the expression (iii), where $E_{slab}$ stands for the total energy of the slab, $N_{Ti}$ corresponds to the number of $TiO_2$ units inside the slab, is the total energy of the corresponding bulk structure per $TiO_2$ unit and finally $S$ correspond to the surface area of the supercell used for the slab.

$$E_{ESFE} = \frac{E_{slab} - N_{Ti}E_{TiO_2-bulk}}{2S} \quad \text{(iii)}$$

It is noteworthy that surface energies cannot be directly compared with our *ESFE*. We are dealing with ultrathin sheets and the *ESFE* values strongly depend on the considered number of $TiO_2$ layers, this is not the case of surface energy where the ESFE would converge with the number of layers. Our objective is to evaluate the relative energy differences for our ultrathin sheets; therefore, *ESFE* is a good option to compare between $TiO_2$ polymorphs.

#### 3.1.1. Anatase and rutile slabs

The observed ESFE values: 0.41 J/m$^2$, 0.64 J/m$^2$ and 0.93 J/m$^2$ for A (1 0 1), A (1 0 0) and A (0 0 1) respectively are in close agreement with the ones reported by Vittadini et al. [37] (0.36 J/m$^2$ for bilayer A (1 0 1), 0.63 J/m$^2$ for three-layer A (1 0 0), and 0.91 J/m$^2$ for five-layer A (0 0 1), referring to the Ti planes as "layers"). These values are highly affected by the degree of the unsaturation of the Ti surface, accompanied by the possibility of the atomic reconstruction at the surface or even in the inner layers. In order to somehow quantify the unsaturation of a given face, the number of "broken bonds" (bb), relative to the bulk coordination (six-fold coordination for titanium atoms, and three-fold coordination for O atoms) can be counted per surface unit as was discussed in a previous work [38]. As can be seen in Table 2, the ESFE follows the general tendency of unsaturation for anatase.

Additionally, it is interesting to observe the reconstruction due to atoms displacements occurred in A (1 0 0) where the Ti atoms belonging to the inner layer move in a way that half of the Ti atoms remain in an octahedral coordination, while the others stand in a distorted hexahedral environment. This is associated with an inward relaxation of the surface oxygen atoms involved. The distance between these oxygen atoms, situated in opposite surface of the slab, changes from 3.78 Å in bulk structure (corresponding with a cell parameter of anatase unit cell) to 3.66 Å in this model. The related O–Ti–O angle varies from 156.5° to 146°, see Fig. 2. This extra unsaturation can reinforce the counted surface unsaturation and thus explaining the relative higher surface energy to unsaturation ratio.

**Table 2**
Surface unsaturation for anatase slabs.

| Slab | ESFE (J/m$^2$) | Unsaturation (bb/Å$^2$) |
|---|---|---|
| A (1 0 1) | 0.41 | 0.103 |
| A (1 0 0) | 0.64 | 0.111 |
| A (0 0 1) | 0.93 | 0.144 |

**Table 3**
Surface unsaturation for rutile slabs.

| Slab | ESFE (J/m$^2$) | Unsaturation (bb/Å$^2$) |
|---|---|---|
| R (1 1 0) | 0.64 | 0.106 |
| R (1 0 0) | 0.66 | 0.149 |
| R (1 0 1) | 1.07 | 0.161 |

Regarding rutile surface energies (or slab formation energies), taking into account the number of layers, the computed values are in agreement with those obtained by Perron et al. [38], which also follows the unsaturation levels (Table 3). No inner changes in coordination were found in this polymorph while the unsatured surface titanium atoms acquire distorted square pyramidal environment.

The fact that *ESFE* calculations gave similar results to surface energy for R (1 1 0) and R (1 0 0) is related to the low dimensionality in the vacuum direction. Since we evaluated the surface energy using ultrathin slabs, the values obtained do not reflect the ones corresponding to macroscopic films previously reported: 0.50 J/m$^2$ for R (1 1 0) and 0.69 J/m$^2$ for R (1 0 0) [38].

#### 3.1.2. $TiO_2$(B) slabs

The structure and stability of $TiO_2$(B) surfaces were previously investigated by Vittadini and coworkers [15]. They found TB (0 0 1) to be the most stable slab (0.40 J/m$^2$) while TB (1 0 0) the least one (0.76 J/m$^2$). Our results, 0.38 J/m$^2$ and 0.83 J/m$^2$ respectively, are in concordance with their observation, which confirms the exceptionally low surface energy of TB (0 0 1) facet in surfaces and ultrathin sheets. This evidence can support the idea of obtaining $TiO_2$(B) related nanostructures experimentally by methods such as hydrothermal treatment of anatase and rutile powders.

For the unsaturation, the broken bonds were counted considering that some of Ti atoms were originally five-fold coordinated in bulk structure and some of the O atoms were two-fold coordinated in addition to the three-fold coordination. Unsaturation values obtained cannot explain the relatively stability in this case (Table 4), as it was previously noticed by Liu et al. [16].

After optimization the bilayer TB (0 0 1) goes into a reconstruction where atoms reach a very symmetrical configuration. Ti atoms which have different environment (octahedral, a square, pyramidal) in bulk present the same square pyramidal geometrical environment, see Fig. 3. This fact appears to act stabilizing this structure in comparison with TB (1 0 0), even though the latter involves lower unsaturation. Note that this structure, as was pointed by Vittadini et al., reminds of the one found by the same

**Table 4**
Surface unsaturation for $TiO_2$(B) slabs.

| Slab | ESFE (J/m$^2$) | Unsaturation (bb/Å$^2$) |
|---|---|---|
| TB (0 0 1) | 0.38 | 0.0879 |
| TB (1 0 0) | 0.83 | 0.0819 |

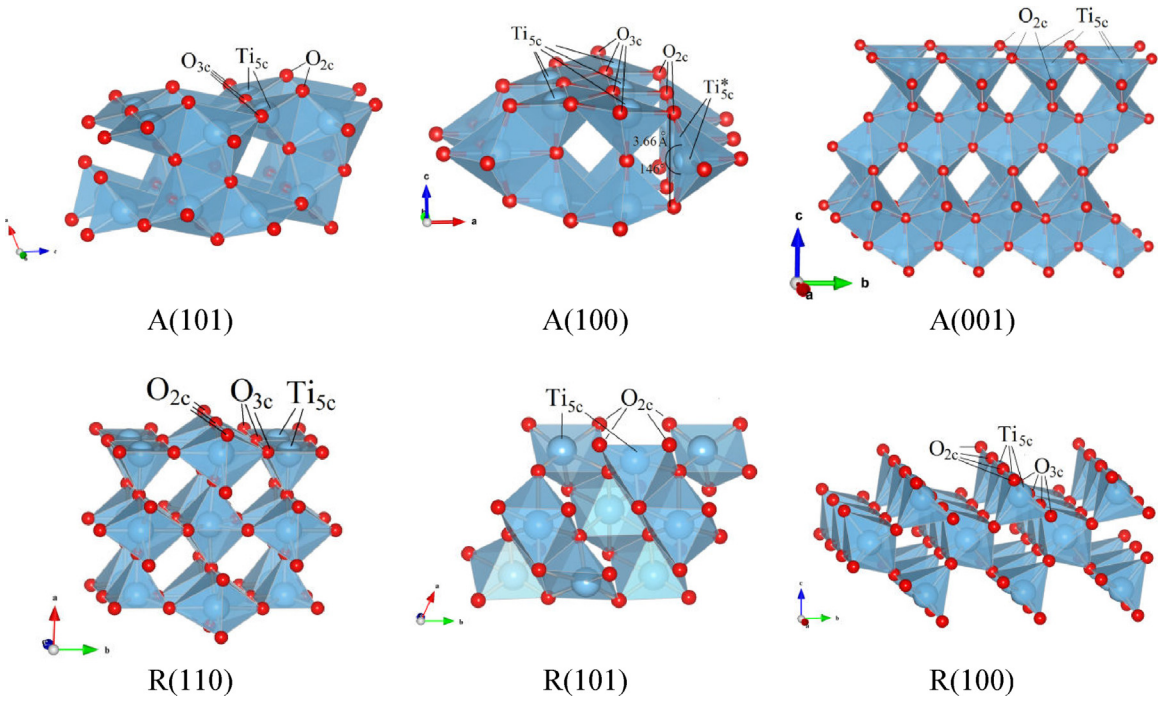


**Fig. 2.** Investigated anatase and rutile slabs after optimizing, being the vacuum direction vertical in all the cases. The figures are presented as supercells for better visualization. The coordination of surface atoms are indicated, *n*c refers to *n*-fold coordination.

group when relaxing anatase A (1 0 1) film with four Ti layers, which was called "pentacoordinated nanosheet", and it was predicted to be the most stable $TiO_2$ nanosheet after lepidocrocite [15,37].

On the other hand, the unsaturated Ti atoms on top of the surface allow the bonding with electron donor species. This point is very important regarding surface reactivity, allowing dyes to be anchored with the semiconductor surface.

### 3.2. Electronic structure of anatase, rutile and $TiO_2$(B) ultrathin sheets

It is not the objective of this work provide detailed calculations on energy gaps and optical properties. The aim is to give a comparative analysis in order to evaluate trends, and thus evaluate in a first instance, the electronic properties of polymorphs and the related ultrathin sheets.

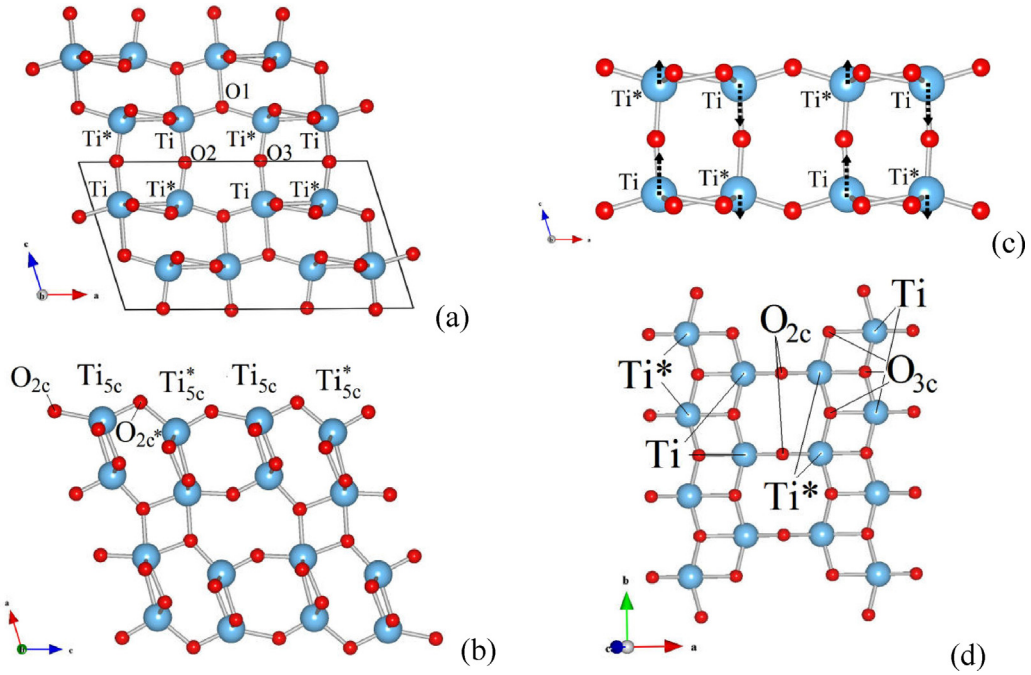


**Fig. 3.** Representation of bulk $TiO_2$(B) (a), TB (1 0 0) (b), and TB (0 0 1) (c) y (d). Ti and Ti* represent octahedral and square pyramidal coordination respectively in bulk structure. In the case of slabs the same notation refers both to $Ti_{5c}$, in which Ti belonged to octahedral environment and Ti* was already five-fold coordinated in bulk.

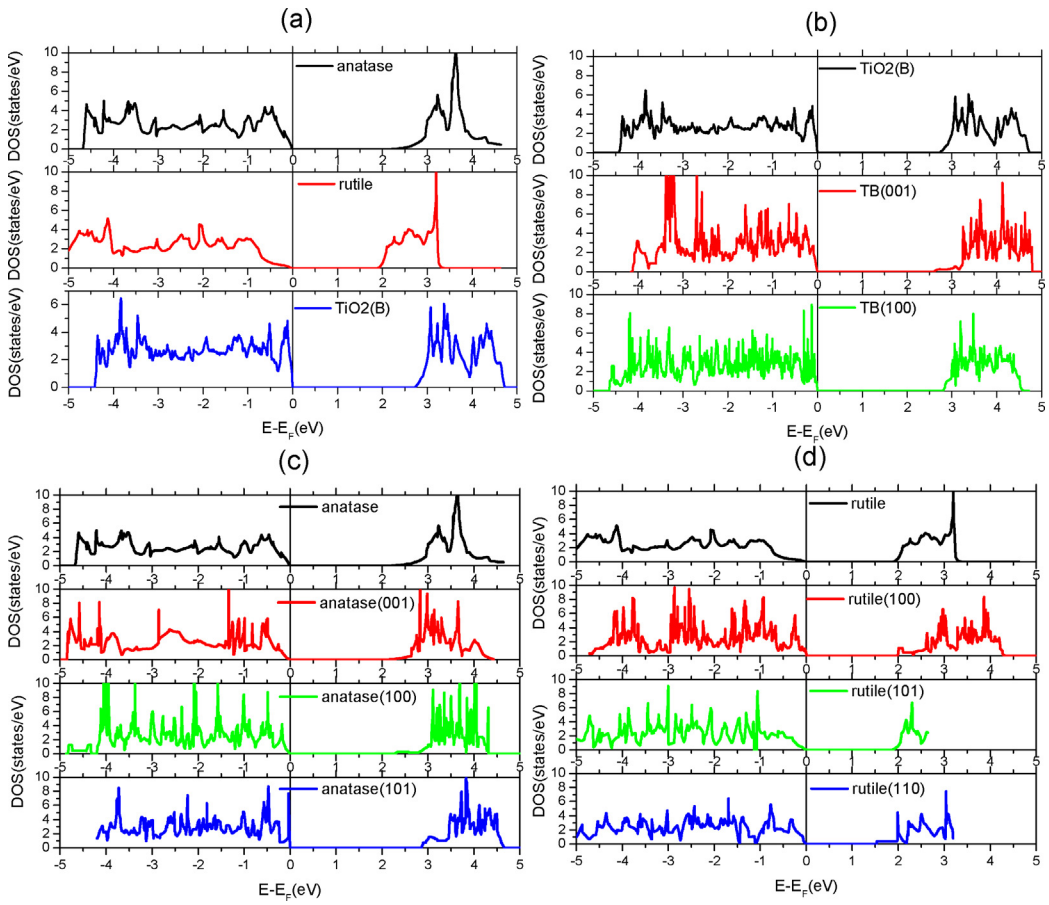


**Fig. 4.** Density of states, per $TiO_2$ units. for (a) bulk structures, (b) $TiO_2$(B) surfaces, (c) anatase surfaces and (d) rutile surfaces.

We obtained the density of electronic states DOS for all the slabs, computing the band gaps at GGA–PBE level, see Table 1 and Fig. 4. In the case of bulk structures we obtained 2.23 eV, 1.90 eV and 2.73 eV for anatase, rutile and $TiO_2$(B) respectively, which agree quite well with other calculations where the energy gaps are 2.30 eV, 1.90 eV [38] and 2.68 eV [14]. The values differ from the experimental ones but following the same trend, with where energy gaps are 3.20 eV, 3.00 eV [39] and 3.22 eV [40], for anatase, rutile and $TiO_2$(B), respectively.

The DOS present an important contribution from O-2p states to the valence band, while conduction band states present major contribution from electronic states with Ti-3d character. This is a well known feature for bulk $TiO_2$ polymorphs, but remains still valid for all the generated ultrathin sheets.

Depending on the site symmetry of the $TiO_n$ ($n$ = 4, 5 or 6) polyhedra and their related connectivity different polymorphs can be obtained, with different features regarding the energy ranges and symmetry decomposition of electronic states (e.g.: the Ti-$t_2g$/Ti-eg peak splitting for electrons in the conduction band of rutile bulk polymorph). It is hard to do this kind of analysis in the case of slabs, due to the low dimensionality of the structures, in which geometric reconstructions leads to lower symmetry and a significant change in the local environment of Ti atoms. The most generalized result is the presence of DOS homogeneous in the region between −5 and 5 eV, with emerging peaks attributed to the under coordinated O atoms proximate to the surface of the slabs.

In the case of $TiO_2$(B) we observe an energy gap of $E_g$ = 2.61 eV and $E_g$ = 2.80 eV for TB (0 0 1) and TB (1 0 0) respectively, which are quite proximate to $E_g$ = 2.40 eV for calculated anatase bulk. While results are in principle promising, further work should be done in order to evaluate its performance as a semiconductor for DSSC, such as molecular levels alignment, suitable energy gaps and favorable thermodynamics for the dye/semiconductor association. This last will be evaluated in the following section.

### 3.3. *Formic acid adsorption on $TiO_2$(B) (0 0 1) and (1 0 0)*

The formic acid adsorption, as it was mentioned before, was studied considering two crystal facets: the major exposed TB (0 0 1) surface together with the minority TB (1 0 0) surface. Due to the bigger reactivity associated with the lower stability, TB (1 0 0) was included in the present analysis since its contribution may not be negligible when evaluating the overall reactivity of $TiO_2$(B) nanoparticles.

The adsorption geometries analyzed for TB (0 0 1) facet are shown in Fig. 5. We follow the notation presented by Vittadini et al. [41], where M denotes monodentate coordination and B refers to bidentate coordination, depending on the number of formic acid oxygen atoms that coordinates with unsaturated surface Ti atoms. MHa is monodentate through the carbonyl group while MHb is monodentate coordination through hydroxyl group. The configurations are classified in non-dissociative and dissociative ones, the latter are indicated with underscore followed by H (M_H and BB_H).

Besides these geometries, another possibility for monodentate molecular adsorption was observed when placing HCOOH molecule initially in a BBH position. In this geometry the H atom from the carbonyl group bonds to a three coordinated O(3c) atom from the surface, see Fig. 6. It is worth noting that, as *cis* conformation was not considered, the H in *trans* molecule was initially pointing towards a surface Ti atom. A rotation of the molecule was observed

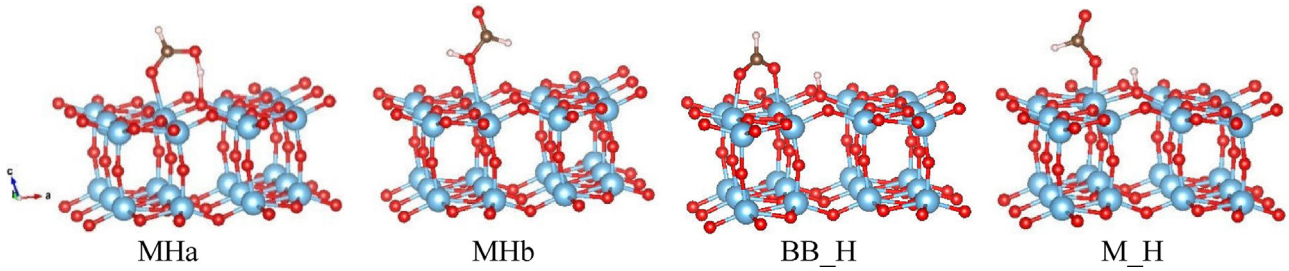


**Fig. 5.** Adsorption geometries which remain stable during the optimization for the TB (0 0 1) slab.

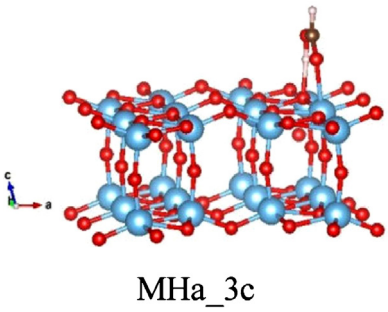


**Fig. 6.** Monodentate adsorption through carbonyl group involving a surface $O_{3c}$.

during the optimization until H finally faces an O atom, no change of molecule conformation occurred.

Regarding M_H dissociative monodentate coordination, it was observed that when the hydrogen of the $HCOO^-$ anions located opposite to the slab, the coordination evolves to a BB_H type, while initially placing the H towards the slab it remains monodentate but poorly stabilized as its negative adsorption energy reflects (Table 5).

$TiO_2$(B) TB (1 0 0) differs from previous orientation in the number of nonequivalent Ti and O surface atoms. This added a new number of interaction options, see Fig. 7.

Results concerning adsorption energy, bond lengths, and molecular angles are listed on Tables 6 and 7. Computed C–O bond lengths correspond to 1.37 Å and 1.22 Å, and the C–O–C angle is 125.4° in case of isolated molecule.

The results show that formic acid is adsorbed in monodentate configuration through carbonyl group (MHa) in dry TB (0 0 1) ultrathin sheet which resembles the adsorption fashion found for anatase A (1 0 1) [41]. On the other hand, in case of TB (1 0 0), a dissociated bridging bidentate geometry (BB_H_2) prevails as occurs onto rutile (1 1 0) surfaces [42].

Regarding the rest of the configurations, on surface TB (0 0 1) the trend in relative stability is the following: BB_H ≥ MHa_3c > MHb > M_H. The difference between the two MHa options is 0.16 eV, while the monodentate through the hydroxyl group differs more significantly in 0.26–0.42 eV. This is in agreement with what was observed for anatase A (1 0 1) [41] and reflects the fact that the oxygen prefers two-fold coordination. Finally, as it was mentioned before, dissociative monodentate configuration is not stabilized.

On surface TB (1 0 0), considering the most stable option of each kind of configuration, the tendency is modified to MHa ≥ M_H > MHb. The fact that M_H is stabilized with respect to MHb could be indicating an enhancement of basicity of surface oxygen atoms. Even more, it is clear the difference in basicity between

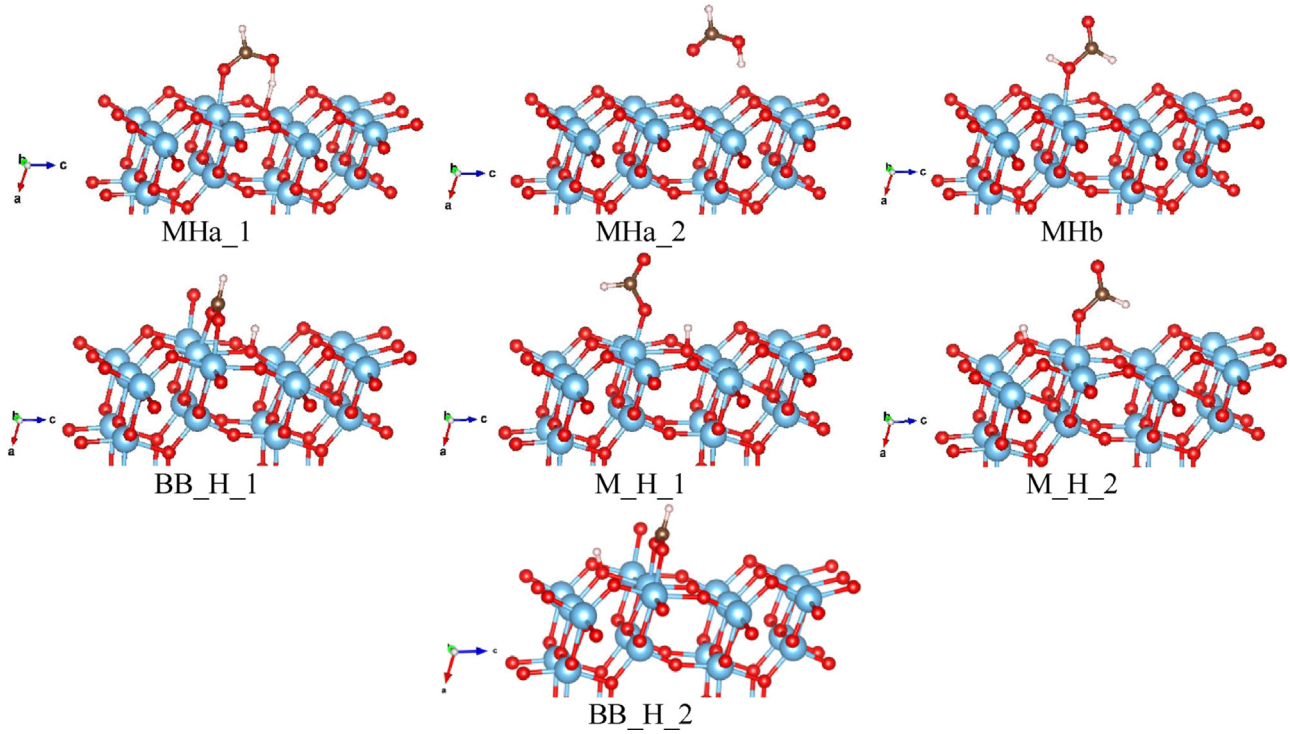


**Fig. 7.** Adsorption geometries which remain stable during the optimization for the TB(1 0 0) slab.

**Table 5**
Adsorption energies, bond distances and bond angles for the different adsorption configurations on **TB (0 0 1)** surface.

| Config. | $E_{ads}$ (eV) | C-O1 (Å) | C-O2 (Å) | $\theta$ (°) | O1-Ti(5c) (Å) | O2-Ti(5c) (Å) | H-O(2c) (Å) |
|---|---|---|---|---|---|---|---|
| MHa | **0.51** | 1.31 | 1.24 | 125.3 | – | 2.35 | 1.57 |
| MHb | **0.09** | 1.37 | 1.21 | 124.0 | 2.64 | – | 2.65* |
| MHa_3c | **0.35** | 1.32 | 1.24 | 125.2 | – | 2.35 | 1.63 |
| M_H | **−0.28** | 1.33 | 1.22 | 124.8 | 2.00 | – | 0.99 |
| *BB_H* | **0.38** | 1.27 | 1.27 | 127.2 | 2.17 | 2.14 | 0.98 |

* This distance is much larger than the conventional hydrogen bond length (1.97 Å).

**Table 6**
Adsorption energies, bond distances and bond angles for the different adsorption configurations on **TB (1 0 0)** surface.

| Config. | Fig. | $E_{ads}$ (eV) | C-O1 (Å) | C-O2 (Å) | $\theta$ (°) | O1-Ti(5c) (Å) | O2-Ti(5c) (Å) | H-O(2c) (Å) |
|---|---|---|---|---|---|---|---|---|
| MHa_1 | 5 | **0.85** | 1.29 | 1.25 | 125.7 | – | 2.15 | 1.48 |
| MHa_2 | 5 | **0.29** | 1.34 | 1.22 | 126.3 | – | 3.99* | 1.83 |
| MHb_1 | 5 | **0.46** | 1.39 | 1.20 | 122.4 | 2.28 | – | 2.46* |
| BB_H_1 | 5 | **1.15** | 1.28 | 1.26 | 127.9 | 2.07 | 2.07 | 0.98 |
| BB_H_2 | 5 | **1.49** | 1.28 | 1.27 | 128.8 | 2.02 | 2.06 | 0.98 |
| M_H_1 | 5 | **0.46** | 1.35 | 1.21 | 123.3 | 1.90 | – | 0.98 |
| *M_H_2* | 5 | **0.81** | 1.36 | 1.21 | 123.3 | 1.87 | – | 0.97 |

* This does not represent a typical Ti–O bond length.
* This distance is much larger than the conventional hydrogen bond length (1.97 Å).

**Table 7**
Adsorption energies (eV), bond distances and bond angles for the different adsorption configurations on **anatase A (1 0 1)** surface.

| Initial Config. | Fig. | $E_{ads}$ (eV) | C-O1 (Å) | C-O2 (Å) | $\theta$ (°) | O1–Ti(5c) (Å) | O2–Ti(5c) (Å) | H–O(2c) (Å) |
|---|---|---|---|---|---|---|---|---|
| MHa_1 | 8 | **0.75** | 1.31 | 1.24 | 125.6 | 2.22 | – | 1.55 |
| MHa_2* | 8 | **0.56** | 1.27 | 1.27 | 128.1 | 2.11 | 2.08 | 0.98 |
| *BB_H* | 8 | **0.56** | 1.27 | 1.27 | 128.1 | 2.11 | 2.08 | 0.98 |

*MHa_2 evolved to BB_H.

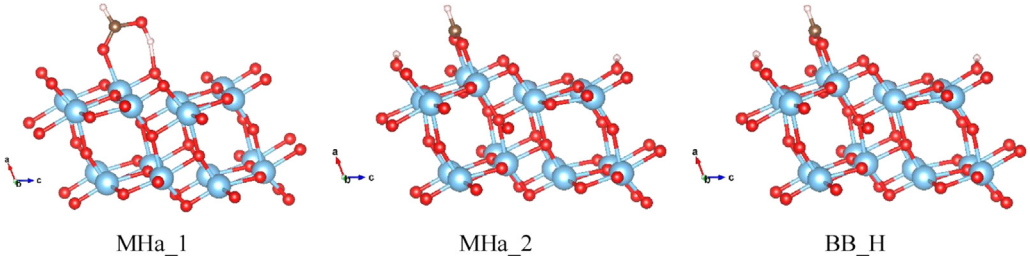


**Fig. 8.** Adsorption geometries evaluated for anatase A (1 0 1) slab.

the two nonequivalent oxygen atoms, since the configuration in which H bonds to $O^*_{2c}$ is about 0.35 eV higher in energy in comparison to H when it bonds to $O_{2c}$. The same difference in energy was found between the two options in bidentate bridging geometries. On the other hand this fact cannot explain the energy difference of about 0.56 eV, computed for the MHa_1 and MHa_2, since in this case the first one is the one which involves de H bonding with $O_{2c}$ and it is the most stable. Clearly what occurs is that the geometry of the surface prevents the oxygen atoms from bonding the Ti atom, where the distance between O(2)–$Ti_{5c}$ is about 3.61 Å. This fact shows that this is not a monodentate coordination but it is a molecule to surface interaction mediated, possibly, by a hydrogen bond.

Finally, the difference in magnitude observed for the analogous configurations changing from TB (0 0 1) to TB (1 0 0) surface, indicates that the increase of energy in the case of the latter allows us to demonstrate the reactivity of this facet, which is in accordance with its lower stability, as discussed before. It is worth noting that our simulation neglects the effect of the hydration of the surface, which can affect the relatively stability among configurations due to the formation of coordination geometries, as was observed by Vittadini et al.in the case of anatase A (1 0 1) [41].

As a final remark, and in order to validate our methodology, the adsorption energies of formic acid in anatase A (1 0 1) for MHa and BB_H configurations (Fig. 8) were computed. Although we found a relatively good agreement regarding the relative stability between the studied configurations, a noticeable difference in the reported value of the adsorption energy was found. In a previous work [41] the reported formation energy corresponds to 0.92 eV for monodentate molecular adsorption (MHa_2) and 0.68 eV for bidentate bridging dissociative configuration, see Table 7.

## 4. Conclusions

The low formation energy for ultrathin $TiO_2$(B) TB (0 0 1) bilayers is comparable with anatase A (1 0 1) which supports the relative stability of this phase at the nanoscale. Thus, it results interesting to study this structure as a possible building block for other high aspect nanostructures such as nanotubes and nanowires.

The comparison between the two facets TB (0 0 1) and TB (1 0 0) showed the less stability of the second one accompanied by a greater reactivity, as expected.

The show that MHa in dry TB (0 0 1) ultrathin sheet and dissociated bridging bidentate geometry (BB_H_2) in the case of TB (1 0 0).

These facts could motivate further work regarding the influence of solvation on the surface reconstruction.

Regarding the reactivity of the semiconductor surfaces, it seems to be adequate for bidentate anchoring of N3 and derived dyes. Considering the optimal distance between the pairs of $Ti_{5c}$ (9.7 Å in TB (0 0 1)), which fits the distance in N3 complex (~9.8 Å). In summary, this work demonstrates the potentiality of $TiO_2$(B) ultrathin sheets as potential semiconductors in DSSC applications.

## Acknowledgments

The authors gratefully acknowledge PEDECIBA, CSIC, ANII – Uruguayan organizations – and Uruguay-INNOVA UE-ANII project for financial support.

## References

[1] X. Chen, S.S. Mao, Titanium dioxide nanomaterials: synthesis, properties, modifications, and applications, Chem. Rev. 107 (7) (2007) 2891–2959, and references therein.
[2] R. Armstrong, G. Armstrong, J. Canales, R. García, P.G. Bruce, Lithium-ion intercalation into $TiO_2$–B nanowires, Adv. Mater. 17 (7) (2005) 862–865.
[3] G. Armstrong, R. Armstrong, P.G. Bruce, P. Reale, B. Scrosati, $TiO_2$(B) nanowires as an improved anode material for lithium-ion batteries containing $LiFePO_4$ or $LiNi_{0.5}Mn_{1.5}O_4$ cathodes and a polymer electrolyte, Adv. Mater. 18 (19) (2006) 2597–2600.
[4] C.-C. Tsai, Y.-Y. Chu, H. Teng, A siple electrophoretic deposition method to prepare $TiO_2$–B nanoribbon thin films for dye-sensitized solar cells, Thin Solid Films 519 (2) (2010) 662–669.
[5] L. Qi, Y. Liu, C. Li, Controlled synthesis of $TiO_2$–B nanowires and nanoparticles for dye-sensitized solar cells, Appl. Surf. Sci. 257 (5) (2010) 1660–1665.
[6] Q. Wang, Z. Wen, J. Li, A hybrid supercapacitor fabricated with a carbon nanotube cathode and a $TiO_2$–B nanowire anode, Adv. Funct. Mater. 16 (16) (2006) 2141–2146.
[7] R. Marchand, L. Brohan, M. Tournox, A new form of titanium dioxide and the potassium octatitanate $K_2Ti_8O_{17}$, Mater. Res. Bull. 15 (8) (1980) 1129–1133.
[8] T.P. Feist, S.J. Mocarski, P.K. Davies, A.J. Jacobson, J.T. Lewandowski, Formation of $TiO_2$(B) by proton exchange and thermolysis of several alkali metal titanate structures, Solid State Ionics 28–30 (1988) 1338–1343.
[9] T.P. Feist, P.K. Davies, The soft chemical synthesis of $TiO_2$(B) from layered titanates, J. Solid State Chem. 101 (1992) 275–295.
[10] T. Kasuga, M. Hiramatsu, A. Hoson, T. Sekino, K. Niihara, Formation of titanium oxide nanotube, Langmuir 14 (1998) 3160–3163.
[11] E. Morgado Jr., M.A.S. de Abreu, O.R.C. Pravia, B.A. Marinkovic, P.M. Jardim, F.C. Rizzo, A.S. Araújo, A study on the structure and thermal stability of titanate nanotubes as a function of sodium content, Solid State Sci. 8 (8) (2006) 888–900.
[12] J. Qu, X.P. Gao, G.R. Li, Q.W. Jiang, T.Y. Yan, Structure transformation and photoelectrochemical properties of TiO2 nanomaterials calcined from titanate nanotubes, J Phys. Chem. C 113 (8) (2009) 3359–3363.
[13] K. Asagoe, S. Ngamsinlapasathian, Y. Suzuki, S. Yoshikawa, Addition of $TiO_2$ nanowires in different polymorphs for dye-sensitized solar cells, Cent. Eur. J. Chem. 5 (2) (2007) 605–619.
[14] M. Ben Yahia, F. Lemoigno, T. Beuvier, J.S. Filhol, M. Richard-Plouet, L. Brohan, M.L. Doublet, Updated references for the structural, electronic and vibrational properties of $TiO_2$(B) bulk using first-principles DFT calculations, J. Chem. Phys. 130 (2009) 204501.
[15] A. Vittadini, M. Casarin, A. Selloni, Structure and stability of $TiO_2$–B surfaces: a density functional study, J. Phys. Chem. C. 113 (44) (2009) 18973–18977.
[16] W. Liu, J.-G. Wang, W. Li, X. Guo, L. Lu, X. Lu, X. Feng, C. Liu, Z. Yang, A shortcut for evaluating activities of $Tio_2$ facets: water dissociative chemisorption on $Tio_2$–B (1 0 0) and (0 0 1), PCCP 12 (31) (2010) 8721–8727.
[17] C. Arrouvel, S.C. Parker, M.S. Islam, Lithium insertion and transport in the $TiO_2$–B anode material: a computational study, Chem. Mater. 21 (20) (2009) 4778–4783.
[18] B.D. Yao, Y.F. Chan, X.Y. Zhang, W.F. Zhang, Z.Y. Yang, N. Wang, Formation mechanism of $TiO_2$ nanotubes, Appl. Phys. Lett. 82 (2) (2003) 281–283.
[19] R. Ma, Y. Bando, T. Sasaki, Nanotubes of lepidocrocite titanates, Chem. Phys. Lett. 380 (2003) 577–582.
[20] T. Gao, Q. Wu, H Fjellvåg, P. Norby, Topological properties of titanate nanotubes, J. Phys. Chem. C 112 (2008) 8548–8552.
[21] T. Sasaki, M. Watanabe, H. Hashizume, H. Yamada, H. Nakazawa, Macromolecule-like aspects for a colloidal suspension of an exfoliated titanate. Pairwise association of nanosheets and dynamic reassembling process initiated from it, J. Am. Chem. Soc. 118 (1996) 8329–8335.
[22] T. Sasaki, M. Watanabe, Semiconductor nanosheet crystallites of quasi-$TiO_2$ and their optical properties, J. Phys. Chem. B 101 (1997) 10159–10161.
[23] R. Ma, K. Fukuda, T. Sasaki, M. Osada, Y. Bando, Structural features of titanate nanotubes/nanobelts revealed by Raman, X-ray absorption Fien structure and electron diffraction characterizations, J. Phys. Chem. B 109 (2005) 6210–6214.
[24] G. Xiang, T. Li, J. Zhuang, X. Wang, Large-scale synthesis of metastable $TiO_2$(B) nanosheets with atomic thickness and their photocatalytic properties, Chem. Commun. 46 (2010) 6801–6803.
[25] S. Liu, H. Jia, L. Han, J. Wang, P. Gao, D. Xu, J. Yang, S. Che, Nanosheet-constructed porous $TiO_2$–B for advanced lithium ion batteries, Adv. Mater. 24 (2012) 3201–3204.
[26] Y.G. Andreev, P.G. Bruce, J. Am. Chem. Soc. 130 (2008) 9931–9934.
[27] E. Morgado Jr., P.M. Jardim, B.A. Marinkovic, F.C. Rizzo, M.A.S. de Abreu, J.L. Zotin, A.S. Araújo, Nanotechnology 18 (2007) 495710–495719.
[28] Dmitry V. Bavykin, Frank C. Walsh, Titanate and Titania Nanotubes Synthesis, Properties and Applications, RSC Publishing, 2010.
[29] P. Hohenberg, W. Kohn, Inhomogeneous electron gas, Phys. Rev. 136 (1964) B864–B871.
[30] W. Kohn, L.J. Sham, Self-consistent equations including exchange and correlation effects, Phys. Rev. 140 (1965) A1133–A1138.
[31] P.E. Blöchl, Projector augmented-wave method, Phys. Rev. B: Condens. Matter 50 (1994) 17953.
[32] G. Kresse, J. Furthmüller, Efficiency of ab-initio total energy calculations for metals and semiconductors using a plane-wave basis set, Comput. Mater. Sci. 6 (1996) 15–50.
[33] G. Kresse, D. Joubert, From ultrasoft pseudopotentials to the projector augmented-wave method, Phys. Rev. B: Condens. Matter 59 (1999) 1758–1775.
[34] J.P. Perdew, K. Burke, M. Ernzerhof, Generalized gradient approximation made simple, Phys. Rev. Lett. 77 (1996) 3865–3868.
[35] J.P. Perdew, K. Burke, M. Ernzerhof, Erratum: generalized gradient approximation made simple, Phys. Rev. Lett. 78 (1997) 1396.
[36] K. Momma, F. Izumi, VESTA 3 for three-dimensional visualization of crystal, volumetric and morphology data, J. Appl. Crystallogr. 44 (2011) 1272–1276.
[37] A. Vittadini, M. Casarin, Ab initio modeling of $TiO_2$ nanosheets, Theor. Chem. Acc. 120 (4–6) (2008) 551–556.
[38] H. Perron, C. Domain, J. Roques, R. Drot, E. Simoni, H. Catalette, Optimisation of accurate rutile $TiO_2$ (1 1 0), (1 0 0), (1 0 1) and (0 0 1) surface models from periodic DFT calculations, Theor. Chem. Acc. 117 (4) (2007) 565–574.
[39] L. Kavan, M. Grätzel, S.E. Gilbert, C. Klemenz, H.J. Scheel, Electrochemical and photoelectrochemical investigation of single-crystal anatase, J. Am. Chem. Soc. 118 (28) (1996) 6716–6723.
[40] G. Betz, H. Tributsch, R. Marchand, Hydrogen insertion (intercalation) and light induced proton exchange at $TiO_2$(B)-electrodes, J. Appl. Electrochem. 14 (3) (1984) 315–322.
[41] A. Vittadini, A. Selloni, F.P. Rotzinger, M.J. Grätzel, Formic acid adsorption on dry and hydrated $TiO_2$ anatase (1 0 1) surfaces by DFT calculations, Phys. Chem. B 104 (6) (2000) 1300–1306, and references therein.
[42] U. Diebold, The surface science of titanium dioxide, Surf. Sci. Rep. 48 (2003) 53–229.